2010 American Control Conference
Marriott Waterfront, Baltimore, MD, USA
June 30-July 02, 2010

Spiral scanning: An alternative to conventional raster scanning in high-speed Scanning Probe Microscopes

I. A. Mahmood and S. O. R. Moheimani

Abstract— **A spiral scanning method for high-speed Atomic Force Microscopy (AFM) is described in this paper. In this method, the sample is scanned in a spiral pattern instead of the conventional raster pattern. A spiral scan can be produced by applying single frequency cosine and sine signals with slowly varying amplitudes to the x axis and y axis of an AFM scanner respectively. The use of the single tone input signals allows the scanner to move at high speeds without exciting the mechanical resonance of the device and with relatively small control efforts. These scan methods can be incorporated into most modern AFMs with minimal effort since they can be implemented in software using the existing hardware. Experimental results obtained by implementing this scanning method on a commercial AFM indicate that the obtained images are of a good quality and the profile of the calibration grating is well captured up to scan frequency of 120 Hz with a scanner where the first resonance frequency is 580 Hz.**

I. Introduction

AFM was invented by Binnig et al. in 1986 [1] based on their design of the scanning tunneling microscopy (STM) [2], [3]. The main use of AFM is for imaging sample surface topography with a very high precision down to the atomic scale. Since its invention, it has emerged as a standard tool in nanotechnology research. This is because it can be used on any sample surfaces and in any environment including air, various gases, vacuum and fluid. Additionally, the AFM can also operate at high and low temperature. The basic components of the AFM include a micro-cantilever with a sharp tip on the free end, a scanner and a laser-photodetector sensor. During operation, the tip of the micro-cantilever is brought very close to the sample surface at a distance of the order of a few nanometers, or less. At such a distance, the interactive forces that exist between the tip and the sample surface change the deflections of the micro-cantilever. These changes in the micro-cantilever are measured using the laser-photodetector sensor [4]. AFM images can be generated by scanning the tip at a constant height over the area of interest on the sample surface. During scan, the measurements from the photodetector will vary according to the sample topographic features. These measurements are recorded and plotted as a function of the scanner's lateral positions to produce an AFM image of the sample surface. Acquisition of the AFM image in this manner is called constant-height mode.

Today, the majority of commercially available AFMs use raster scans to image a sample's surface. A raster scan is performed by moving the scanner along the x axis (fast-axis) in forward and reversed directions (line scan), and then moving the piezoelectric tube along the y axis (slow-axis) in a small step to reach the next line scan. This movement is attained by applying a triangular wave signal to the x axis and a slowly increasing staircase signal to the y axis of the scanner. In order to scan the sample at high speed, a high frequency triangular waveform needs to be used. A drawback of a triangular waveform is that it contains all odd harmonics of the fundamental frequency whose amplitudes attenuate as $1/n^2$, with n being the harmonic number [5]. If a fast triangular waveform is applied to the scanner, the harmonics will inevitably excite the mechanical resonance of the scanner. Consequently, this causes the scanner to vibrate and trace a distorted triangular waveform along the x axis which can significantly distort the generated image. To avoid this complication, the scanning speed of AFMs is often limited to about 10 - 100 times lower then the scanner's first resonance frequency [6].

Recently, there has been significant interest in utilizing feedback control to deal with resonant nature of AFM nanopositioners, e. g. see [7] for an exhaustive overview of the literature, and [8], [9], [10], [11], [12], [13] for further related results. In this approach, a feedback controller is used to flatten the frequency response of the scanner, thus allowing for faster scans. However, as the scan frequency is increased closer to the mechanical bandwidth of the scanner in order to realize high-speed AFM, the positioning precision of the scanner deteriorate considerably. The closed-loop tracking of the triangular waveform typically results in the corners of these waveform to be rounded off and distorted. This is mainly due to the presence of the high frequency harmonics that are outside of the bandwidth of the closed-loop system. Consequently, AFM images generated at high speeds often demonstrate significant distortions especially around the edges of the images.

It should be noted that, recently a few prototype laboratory AFMs have been developed that are capable of imaging a sample at, or close to, video-rates, [14], [15], [16], [17]. Such functionality is particularly important for observing dynamic processes of nanoscale biological specimens, e.g. cells and biopolymers. In order to achieve video rates, using a raster scanned AFM; the scan frequency has to be very high, close to 5 kHz or higher. However to attain such a scan frequency calls for complicated scanner design in order to make the scanner's first resonance frequency much higher than the scan frequency. Additionally, high scanner's first resonance frequency also implies low scan range [18].

I. A. Mahmood and S. O. R. Moheimani are with School of Electrical Engineering and Computer Science, The University of Newcastle, Callaghan, NSW 2308, Australia. Reza.Moheimani@newcastle.edu.au

This paper describes a spiral scanning method for high-speed atomic force microscopy by forcing the scanner to follow a spiral trajectory illustrated in Fig. 1. This pattern is known as the Archimedean spiral. A property of this curve is that its pitch P, which is the distance between two consecutive intersections of the spiral curve with any line passing through the origin, is constant [19]. This property is very important for scanning purposes as it ensures that the sample surface is scanned uniformly. The spiral scanning method proposed in this paper may be a good candidate for video-rates AFMs [14], [15], [16], [17], as the use of the single tone input signals allows the scanners to be designed to have their first resonance frequency much closer to the scan frequency. Hence resulting in relatively simpler scanner design and larger scanning range. It should be pointed out that to operate an AFM at such high scan frequencies one has to overcome other technical challenges, such as the need to utilize very small micro-cantilevers with extremely high resonance frequencies [14].

Spiral scanning method is an alternative to raster-based sinusoidal scan methods that are used to achieve high speed scans in [20] and [21]. In these works, a tuning fork excited at its mechanical resonances and a piezo actuator were used to generate fast scan axis and slow scan axis respectively. In spiral scanning method, both axes follow sinusoidal signals of identical frequencies resulting in a smooth trajectory. This avoids the transient behavior that may occur in sinusoidal scans as the probe moves from one line to the next. Furthermore, the proposed method does not require specialized hardware, e.g. a tuning fork actuator, and can be implemented on a standard AFM with minor software modifications.

Recently the works reported in [22] and [23] have come to our attention, in which the authors, independently, used spiral scanning for AFM. In [22], the frequencies of the sinusoidal input signals applied to a piezoelectric tube scanner were varied with respect to the spiral radius in order to maintain a constant linear velocity over the spiral trajectory. There, the need to use high frequency signals at the center of the spiral trajectory resulted in low scanning speed of the scanner. Nevertheless, the author pointed out that as compared with the raster scan, the use of a smoother trajectory (i.e. spiral trajectory) resulted in relatively faster imaging speed, less distortion on images and lower scanner stress. In [23], a spindle and an x axis slider were used to hold a sample and to mount an AFM head respectively. The rotation of the spindle and the movement of the slider were synchronized in order to scan the sample in a spiral pattern. The main difficulty in using this setup is that the AFM tip needs to be positioned very accurately at the center of the spindle before performing each scan in order to avoid distortion in the center of the scanned images. This appears to be a significant hurdle.

The paper is organized as follows. The generation of input signals to produce the spiral pattern is described in detail in section II. Section III provides descriptions of the AFM and other experimental setups used in this work. Brief descriptions on the modeling and control of the AFM scanner are also included in this section. In section IV experimental results are presented to illustrate the improvement in imaging speed that can be achieved with the spiral scan trajectory. Finally, section V concludes the paper.

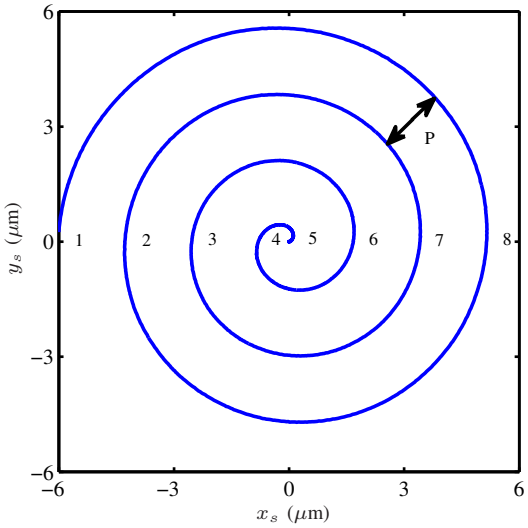

Fig. 1. Spiral scan of 6 μm radius with *number of curves* = 8.

II. Spiral Scan

The equation that generates the spiral of pitch P and traced at an angular velocity of ω can be derived from

$$\frac{dr}{dt} = \frac{P\omega}{2\pi} \tag{1}$$

where r is the instantaneous radius at time t [24]. Equation (1) is solved for r by integrating both sides to obtain

$$r = \frac{P}{2\pi}\omega t \tag{2}$$

for $r = 0$ at $t = 0$. The pitch P is calculated as

$$P = \frac{spiral\ radius \times 2}{number\ of\ curves - 1} \tag{3}$$

where *number of curves* is defined as the number of times the spiral curve crosses through the line $y = 0$. The equation that describes the total scan time t_{total} associated with a spiral scan can be derived by integrating both sides of equation (1) as

$$\int_{r_{start}}^{r_{end}} dr = \frac{P\omega}{2\pi} \int_{t_{start}}^{t_{end}} dt \tag{4}$$

where r_{start} and r_{end} are initial and final values of the spiral radius, and t_{start} and t_{end} are initial and final values of the scan time. From equation (4), if $r_{start} = 0$ at $t_{start} = 0$ and $t_{total} = t_{end} - t_{start}$, we obtain

$$t_{total} = \frac{2\pi r_{end}}{P\omega}. \tag{5}$$

In this work, the spiral scan was implemented using a piezoelectric tube scanner. In order to move the scanner in

a spiral trajectory, equation (2) is transformed into cartesian coordinates. The transformed equations are

$$x_s = r\cos\theta \tag{6}$$

and

$$y_s = r\sin\theta \tag{7}$$

where x_s and y_s are input signals to be applied to the scanner in the x and y axes respectively and $\theta = \omega t$ is the angle. During a scan, since ω is kept constant, this scanning method is also referred to as Constant Angular Velocity (CAV) spiral scan.

It can be inferred from (6) and (7) that, to move the scanner in a spiral trajectory, one only needs to apply slowly varying amplitude single frequency cosine and sine signals to the x- and y-axes of the scanner respectively. The use of the single frequency input signals allows the scanner to be moved at high speed without exciting the mechanical resonance of the scanner. Additionally, closed-loop tracking of these input signals requires smaller control efforts as compared to the tracking of the triangular waveform.

A. Total scan time: Spiral scan vs. Raster scan

A fair comparison of the total scanning time for spiral and raster scans can be made by evaluating the time required for both methods to generate images of equal areas and pitch lengths. The area of a circular spiral scanned image A_{spiral} with a radius of r_{end} can be calculated as

$$A_{spiral} = \pi r_{end}^2. \tag{8}$$

The area of a rectangular raster scanned image A_{raster} can be calculated using

$$A_{raster} = L^2 \tag{9}$$

where L is length of the square image. For both images to have an equal area, equations (8) and (9) are equated to obtain

$$L = \sqrt{\pi} r_{end}. \tag{10}$$

The number of lines in a raster scanned image with pitch P can be calculated as

$$number\ of\ lines = \frac{L}{P} + 1. \tag{11}$$

The total scan time to generate a raster scanned image can be obtained using

$$t_{total\ raster} = \frac{number\ of\ lines}{f} \tag{12}$$

where f is the scan frequency. Thus, by substituting equations (10) and (11) into equation (12), the total scan time for generating a raster scanned image with an area of πr_{end}^2 can be determined as

$$t_{total\_raster} = \frac{\sqrt{\pi} r_{end}}{Pf} + \frac{1}{f}. \tag{13}$$

The total scanning time to generate a spiral scanned image in a CAV mode can be calculated using equation (5) and by substituting $\omega = 2\pi f$ into equation (5),

$$t_{total} = \frac{r_{end}}{Pf}. \tag{14}$$

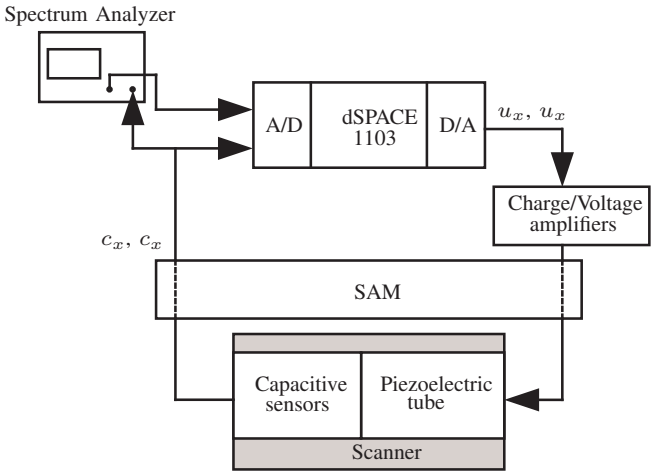

Fig. 2. Block diagram of the experimental setup.

It can be deduced from equations (13) and (14), by ignoring the term $\frac{1}{f}$ in equation (13), for the same scan frequency, an image of equal area and pitch can be generated $\sqrt{\pi}$ (≈ 1.77) times faster using a CAV spiral scan than a raster scan. The reader is alerted that while this is a fair comparison for slow scans, the spiral scanned images tend to be superior to raster scanned images at high scan rates.

III. System description

An experimental setup as illustrated in Fig. 2 was put together in order to investigate the spiral scan capability in generating AFM images. The setup consisted of a commercial NT-MDT Ntegra scanning probe microscope (SPM) fitted with a closed-loop piezoelectric tube scanner. The scanner is incorporated with capacitive displacement sensors that provide measurements of the scanner's displacements in the x, y and z-axes. Two home made DC-accurate charge amplifiers [25] were used to drive the lateral axes of the piezoelectric tube scanner. A dSPACE-1103 rapid prototyping system was used to implement the feedback controllers in real time. The amplifiers and the SPM were interfaced with the dSPACE system using a signal access module (SAM) that allowed direct access to the scanner electrodes. This setup enabled us to directly control the lateral movements of the scanner.

Next, models of the scanner were identified for the purpose of controller design. The scanner is treated as a two single-input single-output (SISO) systems in parallel. The inputs being the voltage signals applied to the charge amplifiers driving $+x$ electrode pair, u_x and $+y$ electrode pair, u_y. The outputs of the system are the scanner displacement measurements from the capacitive sensors in x axis, c_x, and in y axis, c_y. Here, accurate models of the systems were obtained through frequency domain subspace-based system identification approach described in [26]. It is worth mentioning that fairly accurate tracking of the spiral trajectory can be done in open-loop by shaping the input signals. However, closed-loop tracking was undertaken in this work in order

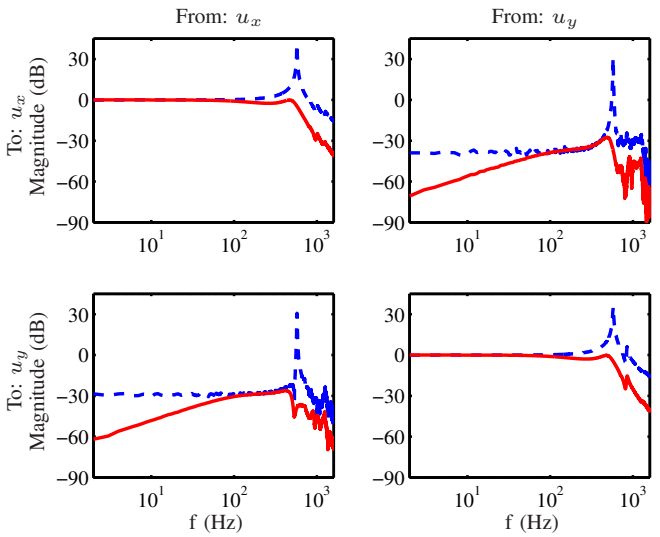

Fig. 3. Open-loop (dash) and closed-loop (solid) frequency responses of the scanner. The resonant behavior of the scanner is improved by over 30 dB due to control action.

to damp the first resonant mode of the piezoelectric tube scanner and to minimize effects such as hysteresis, creep and drift [27]. The overall control structure consists of an inner and an outer loop. The inner loop contains a second order Positive Position Feedback (PPF) [28] controller that works to increase the overall damping of the scanner. The outer loop contains a high-gain integral controller to provide accurate tracking. The procedure that was followed to design these PPF controllers is well documented in reference [29]. Overall, the feedback controllers resulted in a high-bandwidth (540 Hz) closed-loop system as illustrated in Figs. 3.

IV. Results

The performance of the closed-loop systems were then evaluated for high-speed tracking of the CAV spiral. The system was setup to produce spiral scans with $r_{end} = 6.5$ μm and *number of curves* = 512, i.e. the diameter of the resulting circular image consists if 512 pixels. Fig. 4 (a) to (c) illustrate tracking trajectories of the CAV spirals for $\omega_s = 31.4$, 188.5, and 754.0 radians/s. This corresponds to scanning frequencies of $f_s = 5$, 30 and 120 Hz, respectively. In order to allow visual comparison of the tracking trajectories, plots in Fig. 4 (a) to (c) were made to display only the trajectories between ± 0.15 μm. It can be observed that the use of the designed feedback controllers and the shaped input have resulted in excellent tracking performance of the CAV spirals. In order to quantify the tracking performance, the RMS tracking errors between the desired and the achieved trajectories were calculated and are tabulated in Table I. The RMS tracking error is defined as

$$E_{RMS} = \sqrt{\frac{1}{t_{total}} \int_0^{t_{total}} \left(r(t) - r_a(t)\right)^2 dt} \qquad (15)$$

where r is the desired trajectory (or the radius) and $r_a = \sqrt{c_x^2 + c_y^2}$ is the achieved trajectory. Table I shows that E_{RMS} increases as the spiral frequency increases. This increase is mainly due to the inability of the feedback controller to accurately track the rapid changes in the amplitude of the spiral inputs as ω_s is increased. Nevertheless, at $\omega_s =$ 754.0 radians/s, E_{RMS} still remains relatively low, i.e. only 0.1 % of the maximum scanning range (spiral's diameter).

TABLE I

RMS values of tracking error and total scanning time for CAV spiral scans. Images have a resolution of 512 × 512 pixels.

ω_s (radians/s)	E_{rms} (nm)	t_{total} (s)
31.4	3.34	51.10
188.5	9.35	8.52
754.0	14.92	2.13

Having analyzed the performance of the closed-loop system in tracking the CAV spiral, we then moved on to investigate the use of spiral scanning in generating AFM images. The spiral scans were setup to produce images with $r_{end} = 6.5$ μm and *number of curves* = 512, i.e., the diameter of the resulting circular image consists of 512 pixels. A calibration grating NT-MDT TGQ1 with a 20 nm feature-height and a 3 μm period was used as an imaging sample. The AFM was setup to scan the sample in constant-height contact mode using a contact AFM probe with a nominal spring constant of 0.2 N/m and resonance frequency of about 12 kHz. The constant-height contact mode was used here as the commercial AFM controller that controls the vertical positioning of the scanner is not fast enough to track the sample topography for high-speed scans. During each scan, the AFM probe is deflected due to its interactions with the sample. The probe deflection was measured and later used to construct AFM images of the sample topography. Fig. 4 (d) to (f) illustrate AFM images generated using the CAV spiral scans with $\omega_s = 31.4$, 188.5 and 754.0 radians/s.

Fig. 4 (g) to (i) illustrate the cross-section curves of these spiral scanned images at about $y = 0$ μm. The cross-section curves were taken in parallel to the square profile of the calibration grating. Note that, we used the probe deflection measurement of $\omega_s = 31.4$ radians/s, scan to calibrate the probe deflection measurements of other scan frequencies to the height of the calibration grating. This is possible because the probe deflection is very small and thus linear. It can be observed from Fig. 4 (d) to (i) that the obtained images are of a good quality and the lateral and vertical profiles of the calibration grating are well captured. In particular, the images are free from typical distortions caused by tracking errors, scanner vibrations, hysteresis and creep. It is also worth mentioning that the area around the edges of the images was also well imaged. However, during high-speed scans with $\omega_s = 754.0$ radians/s and above, a wave-like artifact can be observed around the outer edges of the AFM images.

Upon a closer examination of the probe deflection signals, we found that the wave-like artifacts were a result of the excitation of the probe's resonance ($\approx$ 12 kHz). Fig. 5

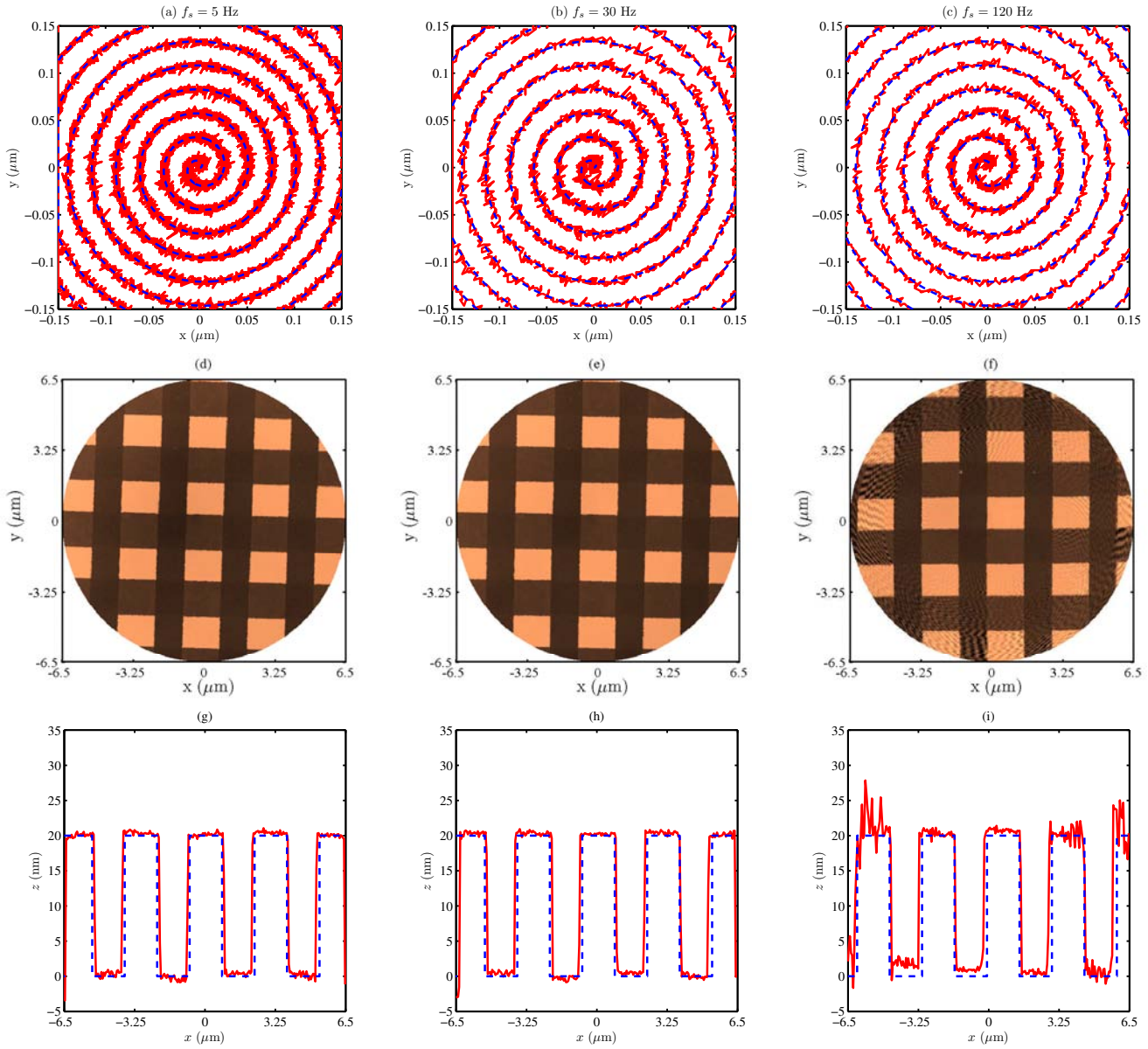

Fig. 4. (a) - (c) Tracking trajectories of CAV spirals between between ± 0.15 μm in closed-loop for $\omega_s = 31.4$, 188.5 and 754.0 radians/s (which corresponds to $f_s = 5$, 30 and 120 Hz). Solid line is the achieved response and dashed line is the desired trajectory. (d) - (f) The corresponding AFM images of NT-MDT TGQ1 grating scanned in constant-height contact mode generated using the CAV spiral. (g) - (i) The corresponding cross-section (solid) and reference (dash) curves of the AFM images illustrated in (d) to (f). The cross-section curves were taken about the center of the AFM images and parallel to the square profile of the calibration grating.

illustrates the probe deflection signals between $r = 5.98$ and 6.00 μm for $\omega_s = 31.4$ and 754.0 radians/s. Fig. 5 (a) shows that during a low-speed scan the probe deflection signal is free of probe's vibrations. However at a high-speed scan, Fig. 5 (b) shows that due to the existence of sharp corners in the topography of the sample, as the probe goes through a full circle, it faces step-like changes that tend to excite its resonance frequency. This effect is much more profound when the sample is scanned at high frequencies. Thus, the image quality can be improved by using a stiffer micro-cantilever. This should allow for much higher scan frequencies, approaching the first resonance of the scanner.

V. Conclusions

In conclusion, in this paper we demonstrated how a spiral scans can be used to obtain AFM images. It is possible to achieve high-speed atomic force microscopy using the spiral scanning, but other issues like the vibrations in the AFM probe need to be considered and addressed. The possibility of using spiral scanning in other SPM applications such as STM should also be explored in the future.

References

[1] G. Binnig, C. F. Quate, and C. Gerber, "Atomic force microscope," *Phys. Rev. Lett.*, vol. 56, no. 9, pp. 930–933, Mar. 1986.

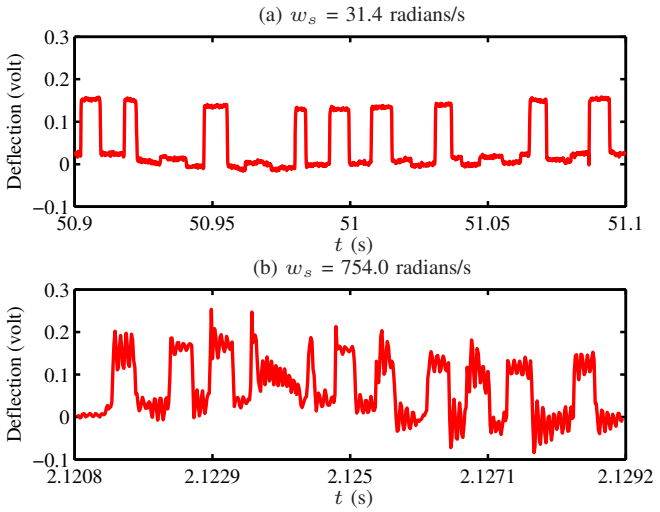

Fig. 5. Probe deflection signals showing the profile of the calibration grating for (a) $\omega_s = 31.4$ radians/s and (b) $f_s = 754.0$ radians/s.

[2] G. Binnig and H. Rohrer, "Scanning tunneling microscopy," *Helv. Phys. Acta*, vol. 55, pp. 726–735, 1982.

[3] G. Binnig, H. Rohrer, C. Gerber, and E. Weibel, "7 x 7 Reconstruction on Si(111) resolved in real space," *Phys. Rev. Lett.*, vol. 50, no. 2, pp. 120–123, Jan. 1983.

[4] E. Meyer, H. J. Hug, and R. Bennewitz, *Scanning probe microscopy*. Springer, 2004.

[5] B. P. Lathi, *Linear systems and signals, 2nd ed*. Oxford University Press, 2004.

[6] D. Croft, G. Shed, and S. Devasia, "Creep, hysteresis, and vibration compensation for piezoactuators: Atomic force microscopy application," *J. Dyn. Sys., Meas., Control*, vol. 123, no. 1, pp. 35 – 43, March 2001.

[7] S. Devasia, E. Eleftheriou, and S. Moheimani, "A survey of control issues in nanopositioning," *Control Systems Technology, IEEE Transactions on*, vol. 15, no. 5, pp. 802 – 823, Sept. 2007.

[8] S. S. Aphale, S. Devasia, and S. O. R. Moheimani, "High-bandwidth control of a piezoelectric nanopositioning stage in the presence of plant uncertainties," *Nanotechnology*, vol. 19, no. 12, p. 125503 (9pp), 2008.

[9] B. Bhikkaji and S. O. R. Moheimani, "Integral resonant control of a piezoelectric tube actuator for fast nanoscale positioning," *Mechatronics, IEEE/ASME Transactions on*, vol. 13, no. 5, pp. 530 – 537, Oct. 2008.

[10] S. Aphale, B. Bhikkaji, and S. Moheimani, "Minimizing scanning errors in piezoelectric stack-actuated nanopositioning platforms," *Nanotechnology, IEEE Transactions on*, vol. 7, no. 1, pp. 79–90, Jan. 2008.

[11] I. Mahmood, S. O. R. Moheimani, and K. Liu, "Tracking control of a nanopositioner using complementary sensors," *Nanotechnology, IEEE Transactions on*, vol. 8, no. 1, pp. 55 – 65, Jan. 2009.

[12] C. Lee and S. M. Salapaka, "Robust broadband nanopositioning: Fundamental trade-offs, analysis, and design in a two-degree-of-freedom control framework," *Nanotechnology*, vol. 20, no. 3, p. 035501 (16pp), 2009.

[13] A. Stemmer, G. Schitter, J. M. Rieber, and F. Allgower, "Control strategies towards faster quantitative imaging in atomic force microscopy," *European Journal of Control*, vol. 11, pp. 4 – 5, 2005.

[14] G. Schitter and M. J. Rost, "Scanning probe microscopy at video-rate," *Materials Today*, vol. 11, no. Supplement 1, pp. 40 – 48, 2008.

[15] T. Ando, T. Uchihashi, and T. Fukuma, "High-speed atomic force microscopy for nano-visualization of dynamic biomolecular processes," *Progress in Surface Science*, vol. 83, no. 7-9, pp. 337 – 437, November 2008.

[16] L. M. Picco, L. Bozec, A. Ulcinas, A. J. Engledew, M. Antognozzi, M. A. Horton, and M. J. Miles, "Breaking the speed limit with atomic force microscopy," *Nanotechnology*, vol. 18, no. 4, p. 044030 (4pp), 2007.

[17] H. Yamashita, K. Voitchovsky, T. Uchihashi, S. A. Contera, R. J. F., and T. Ando, "Dynamics of bacteriorhodopsin 2d crystal observed by high-speed atomic force microscopy," *Journal of Structural Biology*, no. 2, pp. 153 – 158, 2009.

[18] J. H. Kindt, G. E. Fantner, J. A. Cutroni, and P. K. Hansma, "Rigid design of fast scanning probe microscopes using finite element analysis," *Ultramicroscopy*, pp. 259 – 265, 2004.

[19] J. W. Rutter, *Geometry of curves*. Boca Raton: Chapman and Hall/CRC, 2000.

[20] A. D. L. Humphris, J. K. Hobbs, and M. J. Miles, "Ultrahigh-speed scanning near-field optical microscopy capable of over 100 frames per second," *Applied Physics Letters*, vol. 83, no. 1, pp. 6–8, 2003.

[21] A. D. L. Humphris, M. J. Miles, and J. K. Hobbs, "A mechanical microscope: High-speed atomic force microscopy," *Applied Physics Letters*, vol. 86, no. 3, p. 034106, 2005.

[22] S. K. Hung, "Spiral scanning method for atomic force microscopy," in *First International Workshop on TIP-BASED NANOFABRICATION*, Oct. 2008, pp. P–10–1–10.

[23] W. Gao, J. Aoki, B. Ju, and S. Kiyono, "Surface profile measurement of a sinusoidal grid using an atomic force microscope on a diamond turning machine," *Precision Engineering*, pp. 304 – 309, 2007.

[24] A. N. Labinsky, G. A. J. Reynolds, and J. Halliday, "A disk recording system and a method of controlling the rotation of a turn table in such a disk recording system," WO 93/13524, July 2001.

[25] A. J. Fleming and S. O. R. Moheimani, "Sensorless vibration suppression and scan compensation for piezoelectric tube nanopositioners," *Control Systems Technology, IEEE Transactions on*, vol. 14, no. 1, pp. 33 – 44, Jan. 2006.

[26] T. McKelvey, H. Akcay, and L. Ljung, "Subspace-based multivariable system identification from frequency response data," *Automatic Control, IEEE Transactions on*, vol. 41, no. 7, pp. 960 – 979, July 1996.

[27] S. O. R. Moheimani and A. J. Fleming, *Piezoelectric transducers for vibration control and damping*. Germany: Springer, 2006.

[28] J. L. Fanson and T. K. Caughey, "Positive position feedback-control for large space structures," *AIAA Journal*, vol. 28, no. 4, pp. 717 – 724, April 1990.

[29] B. Bhikkaji, M. Ratnam, A. Fleming, and S. Moheimani, "High-performance control of piezoelectric tube scanners," *Control Systems Technology, IEEE Transactions on*, vol. 15, no. 5, pp. 853 – 866, Sept. 2007.